Journal of Ceramic Processing Research. Vol. 13, Special. 1, pp. s47~s51 (2012)

JOURNALOF
Ceramic
Processing Research

Effect of the mechanical properties on the micro-tool performance of Cr-Al-Si-N nanocomposite deposited by hybrid coating method

Jinwoo Sung[a], Suk hoon Shin[a], Tae Jin Je[b], Kwang Ho Kim[a] and Myung Chang Kang[a,]*
[a] *National Core Research Center for Hybrid Materials Solution, Pusan National University, Busan, 609-735, Korea*
[b] *Nano Machining Laboratory, Korea Institute of Machinery and Materials (KIMM), Daejeon, 305-343, Korea*

Comparative studies on mechanical properties and cutting performance of Cr-Al-Si-N coated micro tool for high speed machining applications were performed. Quaternary Cr-Al-Si-N coatings, in which Si was incorporated into Cr-Al-N, were synthesized onto WC-Co substrates using a hybrid system of an arc ion plating (AIP) and DC magnetron sputtering techniques. The high hardness of Cr-Al-Si-N coatings was related to the composite microstructure consisting of fine CrN crystallites and amorphous Si_3N_4. The hardness values of the Cr-Al-Si-N (~55 GPa) coatings were significantly increased compared with those of Cr-Al-N (~24 GPa) coatings. Cutting tests were carried out to evaluate the performances of micro end-mill coated tool in high-speed cutting conditions. Consequently, the quaternary Cr-Al-Si (8.7 at.%)-N coated micro end-mill under dry machining showed good cutting performance in micro end-milling process of AISI D2 work material (HRC 24).

Key words: Hybrid coatings, Cr–Al-Si–N nanocomposite, Microstructure, Microhardness, Tool wear.

Introduction

Micro and nano machining is emerging as a promising fabrication process to meet the dramatically increased needs in making miniature parts in optics, electronics, and biomedical industries. However, in spite of recent advances in micro-tool technology, a micro tool manufacturing and high-speed machining technology are lagging behind [1-3]. The material characteristics of micro-tools with less than 1 mm diameter make their lives very short and unpredictable.

Chromium nitride (CrN) coatings have been widely used as protective coatings for various micro and nano parts, because they have high hardness as well as good wear-resistance due to its low friction coefficient. Recently, ternary Cr-X-N coatings, where X is the alloying element such as Ti, Al, Si, B, C, Ta, Nb, and Ni etc. [4-7], have been actively studied to improve the properties of CrN coatings. Among these ternary systems, Cr-Al-N films have higher hardness (20~30 GPa) than that of CrN coatings, and have much improved oxidation-resistance up to 900 °C due to the formation of stable oxidation barrier of Al_2O_3 layer by migrated aluminum atoms to surface region [8]. Recently, quaternary Cr-Al-Si-N coatings start to be explored since it could become multi-functional coatings having super-hardness (≥40 GPa), excellent oxidation and wear-resistance [9]. Up to now, there is no actual test found in the micro tool applications on the quaternary Cr-Al-Si-N coatings.

In this study, the overall comparison among Cr-Al-N, and Cr-Al-Si-N coatings was performed in terms of microstructure and mechanical properties of these coatings. CrN-based multi-component coatings were deposited on WC-Co substrates by a hybrid coating system of AIP and DC sputtering techniques. The XRD patterns, micro-hardness and HR-TEM were investigated. Cutting tests were carried out to evaluate the performances of micro coated tool under high speed cutting conditions.

Experimental details

Sample preparation and characterization of films

The Cr-Al-N and Cr-Al-Si-N coatings were deposited on WC-Co substrates using the hybrid coating system, where the AIP method was combined with a magnetron sputtering technique. A schematic diagram of apparatus is illustrated in Fig. 1. Arc cathode guns for Cr source and DC sputter gun for the Al and Si sources were loaded on each side of the chamber-wall. A rotational substrate holder was located among the sources. Ar gas (5 N) was introduced into the sputter target holder to increase the sputtering rate and N_2 gas (5 N) was injected near the substrate holder. All Cr, Al and Si targets were 4 N pure. The WC-Co substrates of the disc type (20 mm in diameter and 3 mm in thickness) were cleaned in an ultrasonic cleaner using acetone and alcohol for 20 minutes. The substrates were cleaned again by an ion bombardment using a bias voltage of -600 V under Ar atmosphere of 32 Pa for 15 minutes. The substrates were heated by resistant heaters set inside the chamber, and then the coatings were deposited from arc and

*Corresponding author:
Tel : +82-51-510-2361
Fax: +82-51-518-3360
E-mail: kangmc@pusan.ac.kr

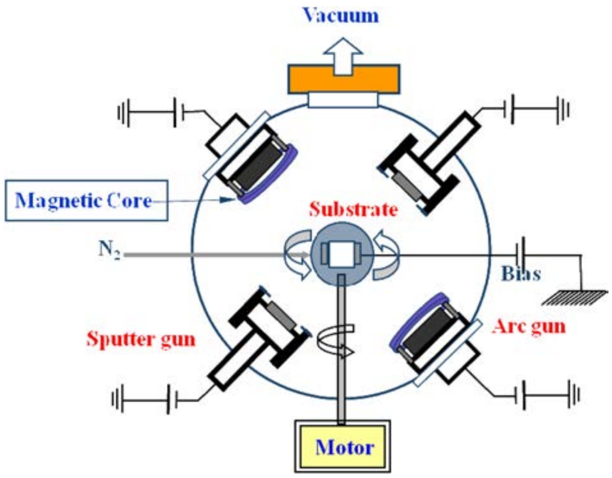

Fg. 1. Measuring method of tool wear values in flank face of micro tool.

Table 1. Typical conditions for Cr-Al-N and Cr-Al-Si–N coatings deposited by the hybrid coating method.

Variable		Cr-Al-N	Cr-Al-Si-N
Arc	Cr target current	55 A	55 A
Sputter	Al target current	1.4 A	1.4 A
	Si target currents		0-2.2 A
N_2 : Ar ratio		2 : 1	
Base pressure		2.7×10^{-3} Pa	
Working pressure		4.0 Pa	
Substrate temperature		300 °C	
Substrate to target distance		300 mm	
Substrate rotation speed		25 rpm	
Typical coatings thickness		~ 2 µm	

sputter sources at a working pressure of 4 Pa. The deposition was performed at the substrate temperature of 300 °C which measured by thermocouple.

Typical deposition conditions for Cr-Al-N and Cr-Al-Si-N coatings by the hybrid coating system are summarized in Table 1. The three kinds of coatings were deposited on WC-Co substrates by a hybrid coatings system. The deposition conditions for Cr-Al-N, and Cr-Al-Si-N coatings were varied by controlling the ratio of CH_4/N_2 gas and Si sputter current. X-ray diffractometer (XRD, Philips, X'Pert-MPD system) using CuKα radiation was used to identify the crystallinity of Cr-Al-N, and Cr-Al-Si-N coatings. The crystallite size in the coating was determined from the direct observation by a field emission-transmission electron microscope (FE-TEM, Jeol, JEM-2010F) operating at 200 kV. The other structural information on the coatings components was obtained from the analyses by the selected area electron diffraction patterns (SAED) and high-resolution transmission electron microscopy (HR-TEM). Micro-hardness measurements were performed using a computer-controlled nano-indentation instrument (MTS, Nano-indentation XP_{II}) equipped with Berkovich diamond indenter under a load of 10 mN.

Cutting test of each tools

As shown in Fig. 2, a series of cutting tests were conducted twice times in the vertical high-speed machining center (Makino, V55) which is attached high-speed air spindle with 120,000 rpm. The rotation precision of the spindle is 1 µm or less. An optimal air pressure condition (0.30-0.55 MPa) was selected for the spindle, which led to the realization of rotation stability. The reliable evaluation system was introduced to identify the cutting performance of coated end-mill tools reported in previous works [10].

An evaluation system, which could sequentially measure the tool wear using one micro-tool, is very useful with respect to measuring time and error. The workpiece used at each experiment is the AISI D2 material enlargement factor of 300 magnifications and an exclusive jig attached on the machine. Each test was started with a fresh micro-tool, and the machining process was stopped at the minimum 0.05 m intervals of cutting length in order to investigate the flank wear. The flank wear width was obtained by average value measured on the flank face (position B) within an axial depth of 20 µm.

Cutting tests of end-mill were evaluated with properties of newly deposited Cr-Al-N, Cr-Al-Si-N coatings. The experimental conditions are presented in Table 2. Hereby, dry cutting defined as the condition where compressed air with 5 kgf/cm^2 pressure is introduced from the nozzle set facing to the cutting position to blow off the cutoffs.

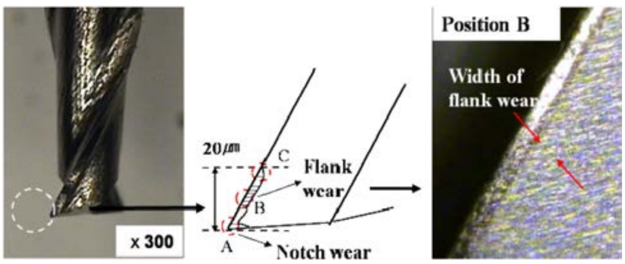

Fig. 2. Measuring method of tool wear value in a flank face of micro tool.

Table 2. Evaluating conditions for micro-tool performance tests.

Tool type	Ø 400 µm, 2-flute end-mill (None, Cr-Al-N, Cr-Al-Si-N coatings)
Work materials	AISI D2 (HRC 24)
Spindle speed [rpm]	40,000, 70,000, 100,000
Feed per tooth [µm/tooth]	2
Radial depth of cut [µm]	20
Axial depth of cut [µm]	20
Cutting type	Down milling
Coolant types	Dry cutting

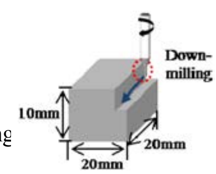

Results and discussion

Characterizations of Cr–Al-Si–N coating layers

Fig. 3 shows the X-ray diffraction patterns of Cr-Al-N and Cr-Al-Si-N films depending on Si contents. Peaks of crystalline Cr-Al-N film are seen with mixed orientations of (111), (200), (220) and (311) crystal planes. As the Si was incorporated into the Cr-Al-N, the peak intensities gradually reduced and the peaks started to disappear over Si content of 12.4 at.%, leading to became amorphous. In addition, the peaks were broadened with an increase of Si content, resulting from the diminution of the grain size or the residual stress induced in the crystal lattice. The progressive change in XRD pattern with Si addition into Cr-Al-N was much similar to the case of Si addition into CrN, i.e., previous reports on nc-CrN/a-Si_3N_4 composites obtained by various deposition techniques [4, 11]. However, a continual shift of XRD peak position was also found with Si addition into Cr-Al-N.

Fig. 4 shows the cross-sectional SAED patterns and dark-field TEM images for Cr-Al-N, Cr-Al-Si (8.7 at.%)-N, and Cr-Al-Si (16.0 at.%)-N coatings. It is seen that the Cr-Al-Si(16 at.%)-N coatings as well as Cr-Al-Si (8.7 at.%)-N are composed of much finer crystallites of CrN and Cr-Al-N, respectively, while the Cr-Al-N coatings have large grains with columnar structure. This microstructural change with Si incorporation into Cr-Al-N is similar to the case of the Si addition into Ti-Al-N, which is previously reported for the nc-(Ti, Al, Si)N/a-Si_3N_4 nanocomposite [3, 12]. The microstructural evolution with Si addition into Cr-Al-N coatings can be also explained with the percolation phenomenon of amorphous phase into Cr-Al-N crystalline phase, as reported earlier for the Cr base materials [13, 14].

Fig. 5 shows the microhardness of Cr-Al-Si-N coatings as depending on Si content. As the Si content increased, the hardness of the Cr-Al-Si-N coatings gradually increased from ~24 GPa of Cr-Al-N, and reached to maximum values of approximately 55 GPa at the Si content of 8.7 at.%, and then drastically decreased with further increase of Si content. These changes are attributed by the microstructural changes for Cr-Al-Si-N coatings with increase of Si content. It can be suggested that the hardness increase of Cr-Al-Si-N coatings up to Si content of 4.5 at.% would be due to the solid solution hardening of crystallites and also the increase of residual stress in coatings induced by a

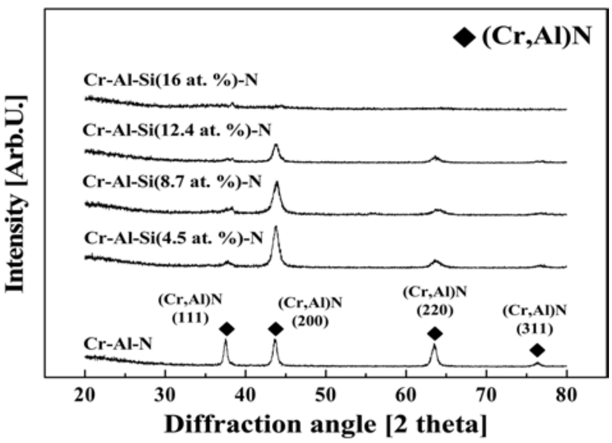

Fig. 3. X-ray diffraction patterns of Cr-Al-Si-N coatings with various Si.

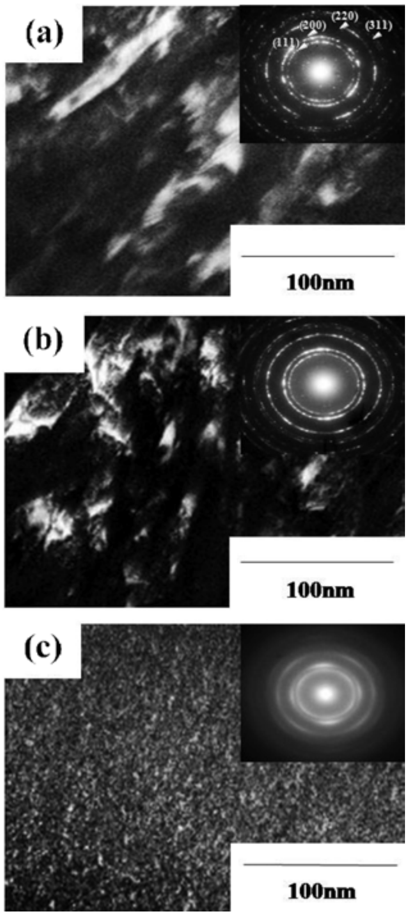

Fig. 4. Cross-sectional SAED patterns and dark-field TEM images. (a) Cr-Al-N, (b) Cr-Al-Si (8.7 at.%)-N, and (c) Cr-Al-Si (16 at.%)-N coatings [13].

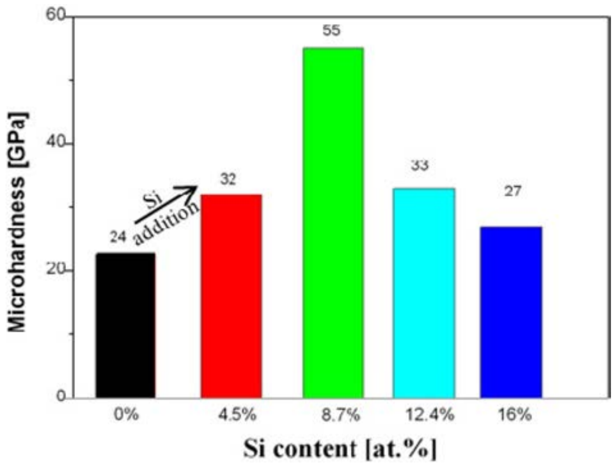

Fig. 5. Microhardness of Cr-Al-N coatings as a function of Si contents.

lattice distortion by the addition of Si. Further increase in hardness of coatings with 8.7 at.% Si would be due to the microstructural changes to a fine composite as well as the solid solution hardening. The coatings with 8.7 at.% Si was previously proved by our instrumental analyses to be a fine composite comprising fine (Cr, Al, Si)N crystallites and amorphous Si_3N_4 [13]. The crystallite size was largely reduced with co-deposition of amorphous Si_3N_4. Thus, the grain boundary hardening by Hall-Petch relationship would take place. Furthermore, the co-deposition of amorphous Si_3N_4 phase among (Cr, Al, Si)N crystallites would enhance cohesive energy of the interphase boundaries [15]. On the other hand, the hardness reduction with further increase of Si content after maximum hardness in Fig. 5 was thought to be due to the increase of volume fraction of amorphous Si_3N_4 phase. It was reported that the increase in volume fraction of amorphous Si_3N_4 phase resulted in the hardness reduction [16].

Performance of Cr–Al-Si–N coating tools

Wear mechanism in general cutting tool is the result of load, friction and high temperature between the cutting edge and the workpiece. When higher cutting temperatures are reached, cutting tool edge can easily lead to chipping and cracking. Accordingly, wear mechanism in high speed machining largely depends on the cutting condition and tool's hardness etc. [3, 10].

In order to evaluate performance of Cr-Al-Si-N coated tool under high speed conditions, five types of coatings were investigated. Fig. 6 shows the relationship between cutting length and tool wear depending on Si contents at various spindle speeds. A typical pattern of wear progression obtained and shown in Fig. 6 is consistent with the pattern reported by others [3, 10, 15]. As expected, with the increase of cutting length and cutting speed, tool wear became shorter for all cutting tools. Overall, the performance of WC-Co tool without coatings was found to be very poor in all spindle speeds. Especially, the wear curve of Cr-Al-Si (8.7 at.%)-N coated tool slightly increased. This trend seemed to be due to higher hardness as shown in Fig. 5. When the spindle speed were 70,000 and 100,000 rpm, as shown in Fig. 6(b) and (c), Cr-Al-Si (4.5 at.%)-N coated tool with the hardness of ~32 GPa was similar to the early tool wear pattern of Cr-Al-Si (16 at.%)-N with ~33 GPa. However, it showed severe wear than the Si content of 16 at.% after the cutting length of 0.3 m in the spindle speed of 70,000 rpm and the cutting length of 0.175 m in the spindle speed of 100,000 rpm. This is why the tribo-layer of SiO_2, $Si(OH)_2$ were easily formed with increase of Si content though Cr-Al-Si (16 at.%)-N coated tool has smaller hardness than Cr-Al-Si (4.5 at%)-N one. Self-lubricating layer like SiO_2, $Si(OH)_2$ reduce the coefficient of friction between the cutting tool and the workpiece, which also reduces cutting temperature in high-speed machining [3, 8]. In addition, Fig. 6(c) shows uncoated, Cr-Al-N(Si : 0 at.%, ~24 GPa) and Cr-Al-Si-N (Si : 8.7 at.%, ~55 GPa) coated tools wear shape taken by a CCD camera when a spindle speed is 100,000 rpm. Cr-Al-Si (8.7 at.%)-N coated tool reached the wear criterion of 12 μm at the cutting length showing stable wear pattern. On the other hand, uncoated and Cr-Al-N coated tool of which hardness was comparatively small, generated partial chipping with increasing of cutting length. And roaring sound and spark were generated during machining. Like this, when the mechanical impact increased as the spindle

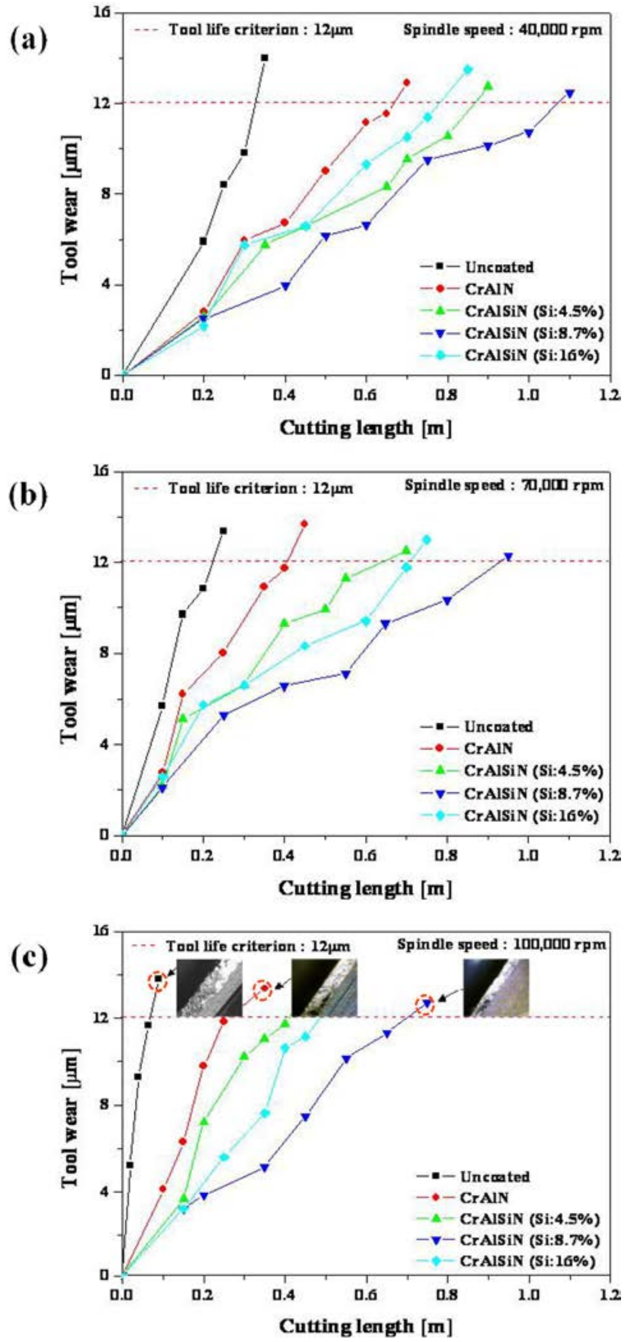

Fig. 6. Tool wear as a function of cutting length at each spindle speeds for uncoated and Cr-Al-Si-N coated tool with various Si contents. (a) 40,000 rpm (b) 70,000 rpm, and (c) 100,000 rpm.

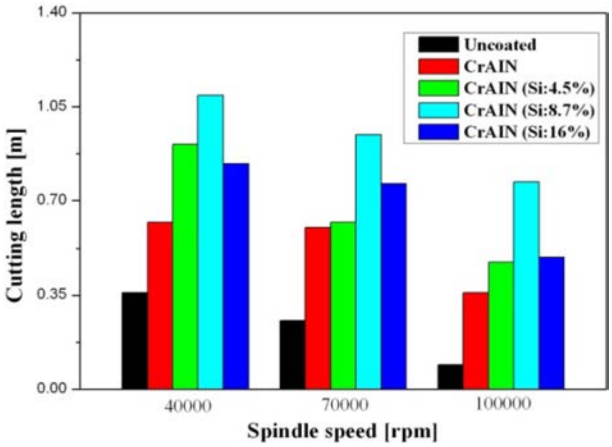

Fig. 7. Comparison of tool life according to Si contents in a series of spindle speed 40,000, 70,000, 100,000 rpm. Tool life criterion is flank wear 12 μm. (Feed per tooth, 2 μm/tooth)

speed increased, flank face showed sever chippings and cracking.

In case of the tool life as a flank wear of 12 μm, Fig. 7 shows that the uncoated, Cr-Al-N, and Cr-Al-Si-N coated micro end-mills are capable of the each cutting length, respectively, before they must be replaced. As the spindle speed increased, the tool life decreased from 20 to 45%. The tool life of Ti-Al-Si (8.7 at.%)-N coated tool was improved 33~200% than others. For high spindle speed 100,000 rpm, the tool life of the Cr-Al-Si (8.7 at.%)-N coated tool were significantly superior to that the uncoated, Cr-Al-N, Cr-Al-Si (4.5 at.%)-N, and Cr-Al-Si (16 at.%)-N tool. The reason for the coated tool with a Si contents of 8.7 at.% would result from the nano-sized crystallites and their uniform distribution embedded in amorphous Si_3N_4 matrix. Thus the hardness plays an active role in the wear process. In case of Ti-Al-Si (4.5 at.%)-N coated tool, tool life was lower 9~13% than Ti-Al-Si (16 at.%)-N except 40,000 rpm. This behavior was that coating layer with Si content of 16 at.% was amorphous and was attributed to the formation of self-lubricating tribo-layers such as SiO_2 or $Si(OH)_2$ for the Si content increase [13, 15]. Consequently, the quaternary Cr-Al-Si (8.7 at.%)-N coated tool under dry cutting showed the excellent cutting performance in micro and high-speed machining of the AISI D2 work material.

Conclusions

Quaternary Cr-Al-Si-N coatings were deposited on WC substrates by the hybrid coating system, where the AIP method was combined with a magnetron sputtering technique. From the XRD and HR-TEM analyses, it could be concluded that the synthesized Cr-Al-Si-N coatings with Si content were nanocomposites consisting of nano-sized (Cr, Al, Si)N crystallites embedded in an amorphous Si_3N_4/SiO_2 matrix. The hardness of Cr-Al-Si-N coatings exhibited the maximum hardness values of 55 GPa at a Si Content of 8.7 at.% due to the microstructural change to a nanocomposite as well as the solid-solution hardening. Tool lives of Ti-Al-Si-N coated tool were abruptly decreased as spindle speed increased. Tool wear pattern of Cr-Al-Si (8.7 at.%)-N coated tool showed considerable stability in this test conditions because of its super-hardness. Consequently, Cr-Al-Si (8.7 at.%)-N coated tool yielded an enhancement tool life of 33~200% compared with the others. This proves the feasibility in the micro and high-speed machining of high hardened materials for industrial applications.

Acknowledgements

This research was supported by the NCRC (National Core Research Center) program through the National Research Foundation of Korea funded by the Ministry of Education, Science and Technology (No. 2010-0001- 226 and 2010-0008-277).

References

1. H. Scheerer, H. Hoche, E. Broszeit, B. Schramm, E. Abele, C. Berger, Surf. Coat. Technol. 200 (2005) 203-207.
2. J.H. Kim, J.H. Hwang and T.Y. Lim, J Ceram Process Res. 10 (2009) 770-773.
3. Y.K. Jeong, M.C. Kang, S.H. Kwon, K.H. Kim, H.G. Kim, and J.S. Kim, Curr Appl. Phys. 9 (2009) 141-144.
4. J. Lin, B. Mishra, S. Myers, P. Ried, and J.J. Moore, J. Nanosci. Nanotechnol. 9 (2009) 3514-3523.
5. S.Q. Wang, L. Chen, B. Yang, K.K. Chang, Y. Du, J. Li, T. Gang, Int. J. of Refractory Met. & Hard Mater. 28 (2010) 593-596.
6. C.L. Chang and C.S. Huang, Thin Solid Films 519 (2011) 4923-4927.
7. T. Miyake, A. Kishimoto and H. Hasegawa, Surf. Coat. Technol. 205 (2010) 290-294.
8. C. Kim, M.C. Kang, J.S. Kim, K.H. Kim, B.S. Shin and T.J. Je, Curr Appl. Phys. 9 (2009) 145-148.
9. D. Mercs, N. Bonasso, S. Naamane, Jean-Michel Bordes, and C. Coddet, Surf. Coat. Technol. 200 (2005) 403.
10. M.C. Kang, J.S. Kim, and K.H. Kim, Surf. Coat. Technol. 200 (2005) 1939-1944.
11. I.W. Park, S.R. Choi, M.H. Lee, and K.H. Kim, J. Vac. Sci. Technol. 21 (2003) 895.
12. S. Carvalho, L. Rebouta, A. Cavaleiro, L.A. Rocha, J. Gomes, and E. Alves, Thin Solid Films 391 (2001) 398-399.
13. I.W. Park, S.R. Choi, M.H. Lee, and K.H. Kim, J. Vac. Sci. Technol. 21 (2003) 895.
14. K.S. Choi, Y.S. Hong, S.H. Kwon, J.W. Choi, Q,M. Wang and K.H. Kim, J Ceram Process Res. 12 (2011) 160-164.
15. D. Rafaja, C, Wustefeld, M. Dopita, M. Ruzicka, V. Klemm, G. Schreiber, D. Heger, and M. Sima, Surf. Coat. Technol. 201 (2007) 9476-9484.
16. S. Veprek, S. Reiprich, L. Shizhi, Appl. Phys. Lett. 66 (1995) 2640.